

Lifetimes and wave functions of ozone metastable vibrational states near the dissociation limit in a full-symmetry approach

David Lapiere,¹ Alexander Alijah,¹ Roman Kochanov,^{2,3} Viatcheslav Kokoouline,⁴ and Vladimir Tyuterev¹

¹*Groupe de Spectrométrie Moléculaire et Atmosphérique, UMR CNRS 7331, University of Reims Champagne-Ardenne, F-51687 Reims Cedex 2, France*

²*Quamer Laboratory, Tomsk State University, Tomsk, Russia*

³*Harvard-Smithsonian Center for Astrophysics Atomic and Molecular Physics Division, MS50 60 Garden Street, Cambridge Massachusetts 02138, USA*

⁴*Department of Physics, University of Central Florida, Orlando, Florida 32816, USA*

(Received 16 July 2016; published 21 October 2016)

Energies and lifetimes (widths) of vibrational states above the lowest dissociation limit of $^{16}\text{O}_3$ were determined using a previously developed efficient approach, which combines hyperspherical coordinates and a complex absorbing potential. The calculations are based on a recently computed potential energy surface of ozone determined with a spectroscopic accuracy [Tyuterev *et al.*, *J. Chem. Phys.* **139**, 134307 (2013)]. The effect of permutational symmetry on rovibrational dynamics and the density of resonance states in O_3 is discussed in detail. Correspondence between quantum numbers appropriate for short- and long-range parts of wave functions of the rovibrational continuum is established. It is shown, by symmetry arguments, that the allowed purely vibrational ($J = 0$) levels of $^{16}\text{O}_3$ and $^{18}\text{O}_3$, both made of bosons with zero nuclear spin, cannot dissociate on the ground-state potential energy surface. Energies and wave functions of bound states of the ozone isotopologue $^{16}\text{O}_3$ with rotational angular momentum $J = 0$ and 1 up to the dissociation threshold were also computed. For bound levels, good agreement with experimental energies is found: The rms deviation between observed and calculated vibrational energies is 1 cm^{-1} . Rotational constants were determined and used for a simple identification of vibrational modes of calculated levels.

DOI: [10.1103/PhysRevA.94.042514](https://doi.org/10.1103/PhysRevA.94.042514)

I. INTRODUCTION

Knowledge of quantum rovibrational states near the dissociation threshold is mandatory for the understanding of the molecular dynamics of formation and depletion processes. In this respect the ozone molecule is a particularly interesting subject for both fundamental molecular physics [1–10] and various applications, owing to the well-known role that this molecule plays in atmospheric physics and climate processes [11,12]. Despite the significant progress made over past decades in the study of ozone spectroscopy [8,13–18] and dynamics [1–6,10,19–30], many aspects of this molecule as well as of the $\text{O}_2 + \text{O}$ complex in high-energy states are not yet fully understood. One of the major motivations for recent investigations of excited ozone has been the discovery of the mass-independent fractionation reported by Mauersberger *et al.* [31–33], Thiemens and Heidenreich [34], and Hippler *et al.* [35] in laboratory and atmospheric experiments: For most molecules, the isotope enrichment scales according to relative mass differences, but the case of ozone shows an extremely marked deviation from this rule. This has been considered as a “milestone in the study of isotope effects” [2] and a “fascinating and surprising aspect ... of selective enrichment of heavy ozone isotopomers” [30]. On the theoretical side, many efforts have been devoted to the interpretation of these findings, in the research groups of Gao and Marcus [20,21], Troe *et al.* [35,36], Grebenshchikov and Schinke [29,37], Babikov *et al.* [28,38], Dawes *et al.* [30] and in many other studies; see [1–6,22–27,39–42] and references therein. Several fundamental issues raised by the ozone studies could have an impact on the understanding of important phenomena in

quantum molecular physics and of the complex energy transfer dynamics near the dissociation threshold.

It has been recognized that a nontrivial account of the symmetry properties [6,39], efficient variational methods for the nuclear motion calculations, and an accurate determination of the full-dimensional ozone potential energy surfaces (PES) are prerequisites for an adequate description of related quantum states and processes in the high-energy range. The ozone molecule exhibits a complex electronic structure and represents a challenge for accurate *ab initio* calculations [7,9,43–48]. Earlier one-dimensional (1D) PES studies predicted an “activation barrier” at the transition state (TS) along the minimum energy path (MEP) [49–51]. Later on more advanced electronic structure calculations have suggested that the MEP shape could have a “reef”-like structure [52–54] with a submerged barrier below the dissociation limit. Following preliminary estimations of Fleurat-Lessard *et al.* [54], this “reef” feature was incorporated into a so-called “hybrid PES” by Babikov *et al.* [38] by introducing a 1D semiempirical correction to the three-dimensional Siebert-Schinke-Bittererova (SSB) [44,45] PES with empirical adjustments to match the experimental dissociation energy. This modified SSB (mSSB) surface containing a shallow van der Waals (vdW) minimum along the dissociation reaction coordinate around $r_1 \sim 4.5\text{--}5.0a_0$ has been used to study the metastable states [38] and also suggested the existence of van der Waals bound states [55–58]. A detailed review of ozone investigations up to this stage has been presented in Schinke *et al.* [1], which concluded that the calculated rate constants were about 3–5 times smaller than the measured ones and had a wrong temperature dependence. Recently, Dawes

et al. [30,59] have argued that an accurate account of several interacting electronic states in the TS region should result in a ground-state potential function without the “reef” feature found in previous *ab initio* calculations. Since this work, and based on scattering studies [5,60,61], the “reef structure” was considered a “deficiency” [62] of the SSB [44,45], the mSSB and similar PES versions [38,63] and was thought to be a plausible reason for the disagreement in rate constant calculations [1,30]. Ndengué *et al.* [62] have reported energies of $J = 0$ and $J = 1$ bound rovibrational ozone states below D_0 using the Dawes *et al.* [59] PES. Variational calculations of the 100 lowest bound vibrational states using that PES resulted in observed minus calculated root-mean-square (obs-calc rms) error [62] of $\sim 20 \text{ cm}^{-1}$ with respect to the experimentally observed band centers of (^{16}O)₃.

In 2013 Tyuterev *et al.* [64] proposed a new analytical representation for the ozone PES accounting for its complicated shape on the way towards the dissociation limit. They constructed two PES versions based on extended *ab initio* calculations. Both PESs were computed at a high level of electronic structure theory with the largest basis sets ever used for ozone. To this end the multi-reference configuration interaction method with Davidson corrections (MRCI+Q) and the full-valence active space was employed using augmented valence atomic basis (AV5Z, AV6Z) followed by the extrapolation to the complete basis set limit. The first PES, referred to as R_PES (“reef_PES”), has been obtained, including a single electronic state in the orbital optimization. It possesses the reef TS feature, as most published potentials do. The second one accounts for Dawes *et al.*’s correction [30], which considers interaction with excited states. This latter potential is referred to as NR_PES (“no_reef_PES”). Both PESs have very similar equilibrium configurations in the bottom of the main C_{2v} potential well and give the same dissociation threshold, very close to recent experimental value of Ruscic $D_0 = 8563 \text{ cm}^{-1}$ [65,66] (as cited in Ref. [47]). Vibrational calculations, using the NR_PES by Tyuterev *et al.* [64], of all (^{16}O)₃ band centers observed in rotationally resolved spectroscopy experiments have resulted in an (rms) obs-calc error of only $\sim 1 \text{ cm}^{-1}$ without any empirical adjustment.

Metastable ozone states above the dissociation threshold are expected to play a key role in the two-step Linderman mechanism [38] of ozone formation at low pressures. They have been studied by Babikov *et al.* [38] and by Grebenshchikov and Schinke [29,37] involving also lifetime calculations. Both investigations are based on SSB or mSSB potential surfaces [38] exhibiting the reef-structure features. Assignment of recent very sensitive cavity-ring-down laser experiments in the TS energy range (from 70% to 93% of D_0) have been possible [8,67–73] due to rovibrational predictions using the NR_PES of Ref. [64] that changed the shape of the bottleneck range along the MEP and transformed the reef into a kind of smooth shoulder. The predictions of bound states with this latter PES in the TS energy range (from 70% to 93% of D_0) exhibit average errors of only 1–2 cm^{-1} for six ozone isotopologues, 666, 668, 686, 868, 886, and 888 [74]. This clearly demonstrated [8] that the NR_PES by Tyuterev *et al.* [64] is much more accurate than other available surfaces for the description of all experimental spectroscopic data, at least up to 8000 cm^{-1} , that is, for bound states up to at least 93% of the dissociation threshold. In

the original publication of Ref. [64], bound states have been computed in the C_{2v} symmetry of the main potential well.

In the present work we report calculations of resonance-state energies, corresponding wave functions, and lifetimes using this PES. Furthermore, bound states near the dissociation threshold are investigated in full D_{3h} symmetry, accounting for possible permutation of identical nuclei over the three potential wells.

II. SYMMETRY CONSIDERATIONS: STATIONARY APPROACH

In the electronic ground state, the ozone molecule has C_{2v} symmetry at equilibrium such that the global potential energy surface has three relatively deep minima, corresponding to three possible arrangements of the oxygen atoms known as “open configurations.” As the barriers between two wells are very high, low-lying rovibrational states of the homonuclear ozone isotopologues, such as (^{16}O)₃, which we study in the present article, may be characterized by irreducible representations (irreps) of the molecular symmetry group $C_{2v}(M)$, which is isomorphic with the C_{2v} point group. In the terminology of Longuet-Higgins [75,76], transformations between the three possible arrangements of three oxygen atoms in ozone are not feasible at low energies.

For weakly bound rovibrational states, however, for which tunneling of the barrier becomes noticeable, and for continuum states of ozone above the barrier, the transformation between arrangements becomes feasible: The description of the dynamics of such states cannot be restricted to one potential well. In this situation, the complete molecular symmetry group must be employed to classify nuclear motion. This group is the three-particle permutation inversion group, $S_3 \times I$. It is isomorphic with the point group D_{3h} and hence may also be designated $D_{3h}(M)$, where M stands for molecular symmetry group [76]. Dissociation of the ozone molecule on the electronic ground-state surface leads to an oxygen atom and a dioxygen molecule, each in its electronic ground state, i.e., $\text{O}(^3P) + \text{O}_2(X^3\Sigma_g^-)$. The symmetry group of the oxygen atom is just the inversion group I , while that of the oxygen molecule is the two-particle permutation inversion group $S_2 \times I$. The latter may be designated $D_{\infty h}(M)$ in order to retain the $D_{\infty h}$ nomenclature for the irreducible representations [77]. In the asymptotic channel, exchange of identical nuclei between the atom and the diatomic molecule becomes unfeasible as their distance goes to infinity. It is clear from this discussion that the molecular symmetry groups $C_{2v}(M)$ and $D_{\infty h}(M)$ are equivalent and just provide different sets of labels for the four irreducible representations. They are two manifestations of the $S_2 \times I$ group. To make this paper self-contained, we give the characters and symmetry labels in Table I. Of the symmetry elements of the point group $D_{\infty h}$, only those are retained for the molecular symmetry group $D_{\infty h}(M)$ that correspond to a permutation inversion operation. This excludes symmetry elements such as $2C(\phi)$, which leave all nuclei on their place. The molecule is placed in the xz plane, which is the convention normally used in ozone spectroscopy [78]. The correspondence of the axes is thus ($x \rightarrow b$, $y \rightarrow c$, $z \rightarrow a$). The transformation properties of the p orbitals, which are needed in the discussion of the asymptotic states, are indicated in the last column of the table.

TABLE I. Character table of the point groups C_{2v} , $D_{\infty h}$ (excerpts), and the permutation inversion group $S_2 \times I$ using the nomenclatures of $C_{2v}(M)$ and $D_{\infty h}(M)$ for the irreducible representations.

C_{2v}		E	C_{2b}	σ_{ab}	σ_{bc}	
$D_{\infty h}$		E	$\infty C_2'$	$\infty \sigma_v$	i	
$S_2 \times I$		E	(12)	E^*	(12)*	
$C_{2v}(M)$	$D_{\infty h}(M)$					
A_1	Σ_g^+	1	1	1	1	$p_b (p_x)$
B_1	Σ_u^+	1	-1	1	-1	$p_a (p_z)$
A_2	Σ_u^-	1	1	-1	-1	
B_2	Σ_g^-	1	-1	-1	1	$p_c (p_y)$

Classification of states in $S_2 \times I$ is convenient for rovibrational states situated deep in the wells, and for the dissociating resonances. We now wish to relate them with the symmetry species of the complete permutation inversion group $S_3 \times I$, or $D_{3h}(M)$. These correlations are shown in Table II. In addition to the symmetry elements of $S_2 \times I$, which are the identity, E , the pair permutation, (12), the inversion of the spatial coordinate system, E^* , and the combination (12)* = (12) \times E^* = $E^* \times$ (12), a new class appears, the cyclic permutations, {(123), (132)}, as well as the class built up by its combination with the inversion of the coordinate system, {(123)*, (132)*}. These new operations describe the exchange between the three localized structures. The correlation presented in Table II is obtained by matching the characters of the common operators, i.e., the identity operation, pair permutations, and the inversion of the coordinate system.

The rovibrational states of ozone may now be classified in the $D_{3h}(M)$ group, allowing for tunneling between the three wells. They can be considered superpositions of the three states localized in their wells, which give rise to a one-dimensional representation and a two-dimensional representation, just as in the case of triplet H_3^+ , which has been discussed before [79]. The energy difference between the one- and the two-dimensional representations is called tunneling splitting. Purely vibrational states have positive parity, i.e., belong to either A_1' , A_2' , or E' , while both prime and double-prime states exist for rotationally excited states. The localized vibrational states to be superimposed may be classified in $C_{2v}(M)$ by the approximate normal mode quantum numbers $|v_1 v_2 v_3\rangle$ of the symmetric stretching vibration, v_1 , the bending vibration, v_2 , and the antisymmetric stretching vibration, v_3 . Since these transform as A_1 , A_1 , and B_1 , respectively, the symmetry of

$|v_1 v_2 v_3\rangle$ is A_1 for v_3 even and B_1 for v_3 odd. In $D_{3h}(M)$, they give rise to the pairs (A_1', E') , (A_1', E') , and (A_2', E') , referring to the one- and two-dimensional representations.

Only those vibrational states that have A_1' symmetry are allowed for the isotopologue $(^{16}O)_3$, as can be seen from the following analysis. The ^{16}O isotope is a boson, with zero nuclear spin; i.e., the total wave function of $(^{16}O)_3$ must be symmetric under exchange of any two ^{16}O nuclei and transform as A_1' or A_1'' in $D_{3h}(M)$. The nuclear spin function transforms as A_1' . Likewise, the electronic wave function of the ground state, X^1A_1 in spectroscopic notation, since the open structure minima have C_{2v} symmetry, is totally symmetric with respect to all nuclear permutations. It means that the rovibrational part of $(^{16}O)_3$ should also be symmetric under an exchange of any two oxygen nuclei, i.e., should transform as the A_1' or the A_1'' irreducible representation. Purely vibrational states have positive parity and thus symmetry A_1' ; the other symmetry species are not allowed. We note in particular that the degenerate tunneling component has zero statistical weight, giving rise to “missing levels” in spectroscopic language. As a consequence, tunneling splitting of the purely vibrational states cannot be observed.

The calculations of the present article were performed in hyperspherical coordinates, as they permit straightforward implementation of the full permutation inversion symmetry. The rovibrational wave function Ψ_v^{Jm} of tunneling ozone can be written as an expansion over products of rotational $\mathcal{R}_{Jkm}(\Omega)$ and vibrational factors $\psi_v^{Jk}(Q)$,

$$\Psi_v^{Jm}(\Omega, Q) = \sum_k \mathcal{R}_{Jkm}(\Omega) \psi_v^{Jk}(Q), \quad (1)$$

where $\mathcal{R}_{Jkm}(\Omega)$ are symmetric top rotational wave functions proportional to the Wigner functions D_{mk}^J

$$\mathcal{R}_{Jkm}(\Omega) = \sqrt{\frac{2J+1}{8\pi^2}} [D_{mk}^J(\Omega)]^*, \quad (2)$$

and depending on the three Euler angles Ω . The vibrational part of the wave function depends on the internal projection k of the angular momentum onto the axis perpendicular to the molecular plane, denoted the y axis in Table I. Note that no decomposition is made here in terms of the $C_{2v}(M)$ normal modes, which would be an approximation.

Each product in expansion (1) should have the same symmetry in the $D_{3h}(M)$ group as the total rovibrational wave function, i.e., A_1' or A_1'' . The symmetry Γ^r of the rotational functions $\mathcal{R}_{Jkm}(\Omega)$ in $D_{3h}(M)$ is well known (see,

TABLE II. Character table of the group $S_3 \times I$ and the relation with the irreducible representations of the group $S_2 \times I$ using the nomenclatures $C_{2v}(M)$ and $D_{\infty h}(M)$.

$S_3 \times I$	E	{(123), (132)}	{(12), (23), (13)}	E^*	{(123)*, (132)*}	{(12)*, (23)*, (13)*}	$S_2 \times I$	
							$C_{2v}(M)$	$D_{\infty h}(M)$
$D_{3h}(M)$								
A_1'	1	1	1	1	1	1	A_1	Σ_g^+
A_2'	1	1	-1	1	1	-1	B_1	Σ_u^+
E'	2	-1	0	2	-1	0	$A_1 + B_1$	$\Sigma_g^+ + \Sigma_u^+$
A_1''	1	1	1	-1	-1	-1	A_2	Σ_u^-
A_2''	1	1	-1	-1	-1	1	B_2	Σ_g^-
E''	2	-1	0	-2	1	0	$A_2 + B_2$	$\Sigma_u^- + \Sigma_g^-$

TABLE III. Allowed combinations of irreducible representations of the rotational and vibrational factors in the expansion of Eq. (1).^a

J	0	1	1	2	2	2	3	3	3	3
k	0	0	± 1	0	± 1	± 2	0	± 1	± 2	$\pm 3^*$
Γ^r	A'_1	A'_2	E''	A'_1	E''	E'	A'_2	E''	E'	A''_1, A''_2
Γ^v	A'_1	A'_2	E'	A'_1	E''	E'	A'_2	E'	E'	A'_1, A'_2
$\Gamma^r \times \Gamma^v$	A'_1	A'_1	A''_1	A'_1	A'_1	A'_1	A'_1	A''_1	A'_1	A''_1, A''_2

^aThe symmetrized combinations of functions with $k = \pm 3$ transform as the A''_1 and A''_2 representations in $D_{3h}(M)$. The direct products, $\Gamma^r \times \Gamma^v$, of two E representations yield $A_1 + A_2 + E$ and contain the A_1 representation. Only the latter is listed in the last line of the table. The parity is given by the usual rule ' \times ' = ', '' \times ' = ', ' \times ' = ', '' \times ' = ''.

for example, [76,80]). It imposes restrictions on the possible irreducible representations of the vibrational factors $\psi_v^{jk}(Q)$: The rotational and vibrational wave functions should be of the same species, both A_1 , or both A_2 , or both E . Parities of the wave functions are not restricted. The parity of the vibrational functions is always positive; the parity of the rotational function is positive for even k and negative for odd k . Examples of the irreducible representations of rotational and vibrational functions are given in Table III for $J \leq 3$.

Let us now turn to the symmetry classification of the wave functions of the decaying resonance states. The lowest dissociation limit of ozone produces the oxygen atom, $O(^3P)$, and the oxygen molecule, $O_2(X^3\Sigma_g^-)$, in their electronic ground states. The orbital degeneracy of the atomic P state is three. One orbital is oriented perpendicular to the plane spanned by the three nuclei, denoted as p_c in Table I. According to Table II, it transforms as A''_2 in $D_{3h}(M)$. The two in-plane orbitals transform as E' . On the other hand, the electronic symmetry of the dioxygen molecule is Σ_g^- in $D_{\infty h}(M)$ or A''_2 in $D_{3h}(M)$. At large distances, the electronic ground state, X^1A_1 , of ozone correlates with the perpendicular (p_c) component of the atomic P state plus the diatomic Σ_g^- state, each of which has A''_2 symmetry in $D_{3h}(M)$ such that their product is indeed A'_1 .

The electronic ground state of O_2 is antisymmetric with respect to an exchange of the two nuclei. Since the vibrational states of O_2 are totally symmetric, this implies that the rotational functions must be antisymmetric to yield a symmetric nuclear wave function. The rotational functions of O_2 transform as Σ_g^+ for even values of j and as Σ_g^- for odd values. Rotational states of $^{16}O_2$ must therefore have odd rotational angular momentum, j , and the lowest rovibrational state is ($v = 0, j = 1$).

Let us now analyze the asymptotic wave function in the exit channel κ with $\kappa = 1, 2, 3$. It can be expanded as

$$\Psi_{\kappa v_d j l}^{Jm}(\vec{r}_\kappa, \vec{R}_\kappa) \approx \frac{1}{r_\kappa R_\kappa} \varphi_a^{el} \varphi_d^{el} \chi_{v_d j}(r_\kappa) \mathcal{Y}_{jl}^{Jm}(\hat{r}_\kappa, \hat{R}_\kappa) e^{i(kR_\kappa - l\pi/2)}, \quad (3)$$

where $\exp[i(kR_\kappa - l\pi/2)]$ is the scattering function of the outgoing wave and $\chi_{v_d j}(r_\kappa)$ the vibrational wave function of the O_2 molecule; r_κ and R_κ are the true, not mass-scaled, distances in the Jacobi coordinate system κ . \hat{r} denotes the two angles that describe the rotation of the O_2 molecule in the

laboratory coordinate system, and \hat{R} the angles of the direction, with respect to the laboratory coordinate system, of the outgoing oxygen atom. Functions φ_a^{el} and φ_d^{el} represent electronic states of the $O(P)$ atom and the $O_2(X^3\Sigma_g^+)$ molecule. Angular momenta of the atom-diatom relative motion, l , and of the rotation of the oxygen molecule, j , must be coupled to yield the total angular momentum, J , which is taken care of by the bipolar harmonics, \mathcal{Y}_{jl}^{Jm} . They are defined as

$$\mathcal{Y}_{jl}^{Jm}(\hat{r}_\kappa, \hat{R}_\kappa) = \sum_{m_l, m_j} C_{j m_l m_j}^{J m} Y_{j m_l}(\hat{r}_\kappa) Y_{l m_j}(\hat{R}_\kappa), \quad (4)$$

where the Y are spherical harmonics and C are Clebsch-Gordan coefficients. The scattering function in Eq. (3) is not symmetric with respect to permutation of three bosonic nuclei and, therefore, cannot be correlated in this form with the short-distance form of Eq. (1), which does have correct symmetry behavior (for the combinations of quantum numbers given in Table III). To bring the function of Eq. (3) to the form satisfying the permutational symmetry of three bosons, in the language of group theory, one has to apply projectors of the $D_{3h}(M)$ group of the two allowed irreducible representations, A'_1 or A''_1 . An efficient way to perform it is to use a general approach of Ref. [81] applicable to a three-body system with arbitrary total nuclear spin. Equations (19) of that reference do not take into account the electronic part of the total wave function. The electronic wave function of the dioxygen φ_d^{el} changes sign under permutation of the two atoms and under the inversion operation, and the atomic φ_a^{el} changes sign under the inversion only. Therefore, Eqs. (19) of Ref. [81] take the following form for the present case:

$$(12)\Psi_{\kappa v_d j l}^{Jm}(\vec{r}_\kappa, \vec{R}_\kappa) = (-1)^{j+1} \Psi_{\kappa v_d j l}^{Jm}(\vec{r}_\kappa, \vec{R}_\kappa), \\ E^* \Psi_{\kappa v_d j l}^{Jm}(\vec{r}_\kappa, \vec{R}_\kappa) = (-1)^{l+j} \Psi_{\kappa v_d j l}^{Jm}(\vec{r}_\kappa, \vec{R}_\kappa). \quad (5)$$

With these properties, the projectors P_Γ take the form (see Eqs. (20) of Ref. [81])

$$P_\Gamma \Psi_{\kappa v_d j l}^{Jm}(\vec{r}_\kappa, \vec{R}_\kappa) \\ = [1 + \chi_{23}^\Gamma(23) + \chi_{31}^\Gamma(31)] [1 + (-1)^{j+1} \chi_{12}^\Gamma] \\ \times [1 + (-1)^{l+j} \chi_{E^*}^\Gamma] \Psi_{\kappa v_d j l}^{Jm}(\vec{r}_\kappa, \vec{R}_\kappa), \quad (6)$$

for any of the $D_{3h}(M)$ representations. Here χ^Γ are characters of the representation Γ given in Table II. From the expression in the second parentheses on the right side of the equation above, it is clear that for the allowed representations A'_1 and A''_1 , if j is even, the projectors are identically zero: $P_{A'_1} = 0, P_{A''_1} = 0$. This simply means that a free molecule $^{16}O_2(X^3\Sigma_g^+)$ can only have odd rotational angular momentum j . The expression in the third parentheses means that if the quantum numbers l and j have different parity, the projectors again give identically zero for A'_1 (but not for A''_1). In particular, it implies that dissociative states of $^{16}O_3$ with rotational angular momentum $J = 0$ do not exist within the adiabatic approximation.

III. NUCLEAR DYNAMICS

The present, stationary theoretical approach to describe nuclear dynamics was developed previously by Kokooouline *et al.* [79,82–84]. It is based on the two-step procedure of

solving the stationary Schrödinger equation in hyperspherical coordinates [85–87]. Although the method was previously applied to several three-body problems, it has never been applied to a system with large masses of the three particles and so many bound states: In Ref. [83] the method was developed and tested on a benchmark system of a three-boson nucleus with a very shallow potential supporting only one bound state and one resonance. In Ref. [84], the method was employed to calculate resonances in three-body collisions of hydrogen atoms. The lowest H_3 potential energy surface has two coupled sheets without any bound state but with many resonances. The method was also routinely used to represent the vibrational continuum in studies of dissociate recombination of isotopologues of H_3^+ [88,89]. An important difference of the present study with the previous ones is that the number of bound states is large, which requires a significantly larger basis to represent the vibrational dynamics near and above the dissociation.

We briefly summarize the main elements of the approach. To solve the Schrödinger equation

$$[T(\rho, \theta, \phi) + V(\rho, \theta, \phi)]\Phi_v(\rho, \theta, \phi) = E_v \Phi_v(\rho, \theta, \phi) \quad (7)$$

for three particles interacting through the potential $V(\rho, \theta, \phi)$ in the hyperspherical coordinates ρ , θ , and ϕ , first, the adiabatic hyperspherical curves $U_a(\rho)$ and the corresponding hyperangular eigenstates $\varphi_a(\rho_j; \theta, \phi)$ [hyperspherical adiabatic states (HSAs)] are obtained by solving the equation in the two-dimensional space of the hyperangles θ and ϕ for several fixed values of the hyperradius ρ_j ($j = 1, 2, \dots$); i.e., the following equation is solved:

$$\left[\hbar^2 \frac{\Lambda^2 + \frac{15}{4}}{2\mu\rho_j^2} + V(\rho_j; \theta, \phi) \right] \varphi_a(\rho_j; \theta, \phi) = U_a(\rho_j) \varphi_a(\rho_j; \theta, \phi). \quad (8)$$

In the above equation, Λ^2 is the grand angular momentum squared [87,90] and μ is the three-particle reduced mass: For identical oxygen atoms with mass m_O , one has $\mu = m_O/\sqrt{3}$. The equation is solved using the approach described in Ref. [91]. The solution of Eq. (8) yields adiabatic curves $U_a(\rho)$ and eigenfunctions $\varphi_a(\rho; \theta, \phi)$, defining a set of HSA channels a . The HSA states are then used to expand the wave function Φ_v in Eq. (7)

$$\Phi_v(\mathcal{Q}) = \sum_a \psi_a(\rho_j) \varphi_a(\rho_j; \theta, \phi). \quad (9)$$

The expansion coefficients $\psi_a(\rho_i)$ depend on hyperradius ρ . Following the original idea of Ref. [92] the hyperradial wave functions $\psi_a(\rho_i)$ are then expanded in the discrete variable representation (DVR) basis $\pi_j(\rho)$

$$\psi_a(\rho) = \sum_j c_{j,a} \pi_j(\rho). \quad (10)$$

Inserting the two above expansions into the initial Schrödinger equation (7), one obtains

$$\sum_{j', a'} \left[\langle \pi_{j'} | -\frac{\hbar^2}{2\mu} \frac{d^2}{d\rho^2} | \pi_j \rangle \mathcal{O}_{j' a', j a} + U_a(\rho_j) \delta_{j', j} \delta_{a' a} \right] c_{j' a'} = E \sum_{a'} \mathcal{O}_{j a', j a} c_{j a'}, \quad (11)$$

with

$$\mathcal{O}_{j' a', j a} = \langle \varphi_{a'}(\rho_{j'}; \theta, \phi) | \varphi_a(\rho_j; \theta, \phi) \rangle. \quad (12)$$

In the above equation, the matrix elements of the second-order derivative with respect to ρ is calculated analytically (see, for example, [93,94] and references therein).

The described approach of solving the Schrödinger equation using the adiabatic (HSA) basis replaces the usual form of nonadiabatic couplings in terms of derivatives with respect to ρ with overlaps between adiabatic states $\varphi_a(\rho, \theta, \phi)$ evaluated at different values of ρ . The approach is particularly advantageous here, since the adiabaticity of the hyperradial motion, when separated from hyperangular motion, is not satisfactory, so that multiple avoided crossings between HSA energies $U_a(\rho)$ occur. This is the usual situation in three-body dynamics. Representing nonadiabatic couplings by derivatives $\langle \varphi_{a'} | \partial/\partial\rho | \varphi_a \rangle$ and $\langle \varphi_{a'} | \partial^2/\partial\rho^2 | \varphi_a \rangle$ near the avoided crossings would require a very small grid step in ρ . The use of overlaps between HSA states reduces significantly the number of grid points along ρ required for accurate representation of vibrational dynamics.

In Ref. [64], the main features of the PES were demonstrated in internal coordinates. In the present study, the NR_PES of Ref. [64], which had been originally defined in the C_{2v} wells, was symmetrized according to the nuclear permutations and converted in the hyperspherical coordinates [85–87]. Figure 1 shows the PES as a function of the two hyperangles for several values of the hyperradius. As evident from the plot at $\rho = 5.4$ bohrs the potential barrier between the wells is situated at energies 9000 cm^{-1} , i.e., very close to the dissociation threshold. The passage between the wells occurs at geometries beyond the “shoulder” of the ozone potential. Therefore, one expects weakly bound low-energy resonances delocalized between the three potential wells. To represent nuclear dynamics of such near-dissociation levels, one needs to take into account

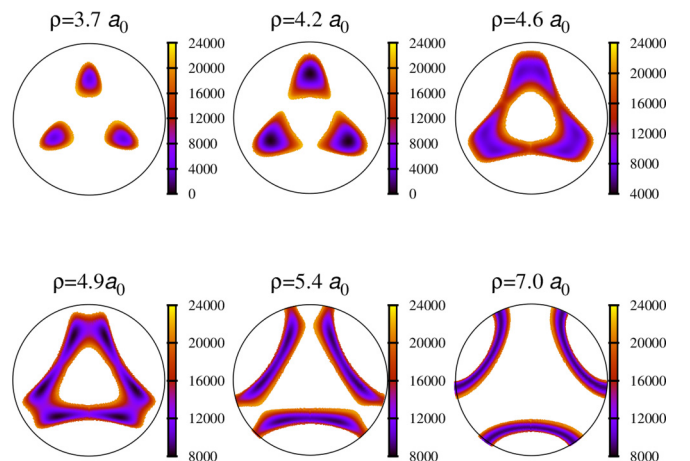


FIG. 1. Ozone potential energy surface (NR_PES of Ref. [64]) as a function of the two hyperangles for several values of the hyperradius. In the plots, the hyperangles are represented in a polar coordinate system (see Fig. 6 of Ref. [80]): θ increases from the center of each plot to its edge; ϕ is a cyclic variable (polar angle) changing from 0 to 2π . The minimum of PES, situated near $\rho = 4.2a_0$, is chosen as the origin. The electronic energy of dissociation to the atom and the diatomic molecule at equilibrium is at 9164 cm^{-1} .

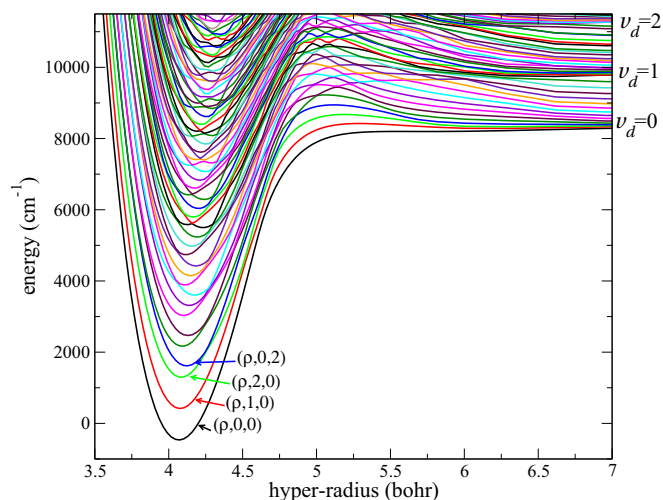


FIG. 2. Hyperspherical adiabatic curves $U_a(\rho)$ of the A_1 irreducible representation and $J = 0$ as a function of hyperradius obtained for $^{16}\text{O}_3$. In this figure, the energy origin is chosen at the ground vibrational level of $^{16}\text{O}_3$, situated 1443.524 cm^{-1} above the PES minimum. The $v_d = 0, 1, 2$ labels indicate energies of the $\text{O} + \text{O}_2$ (v_d) asymptotic vibrational channels. Multiple HSA curves between the vibrational channels correspond to various rotational channels j of the dissociating oxygen molecule. For the A_1 vibrational states, only even j are allowed. Because $J = 0$, the partial wave in each asymptotic channel (v_d, j, l) is determined simply as $l = j$.

the three potential wells simultaneously. The energy D_0 of dissociation to the $^{16}\text{O}(^3P)$ and $^{16}\text{O}_2(X^3\Sigma_g^- [v_d = 0, j = 0])$ products, computed on the PES of Ref. [64], is 8555 cm^{-1} above the ground rovibrational level of $^{16}\text{O}_3$. This is even closer to the experimental $D_0 = 8563\text{ cm}^{-1}$ value by Ruscic [65,66,47] than the estimation of the original work [64] because the zero-point energy of the O_2 fragment was treated here in a more consistent way using the same global PES

A convenient way of analyzing nuclear dynamics of three atoms is given by HSA curves, which could be viewed in a way similar to Born-Oppenheimer curves for diatomic molecules, except that the adiabatic and dissociation coordinate in the HSA curves is the hyperradius, not the interatomic distance. In contrast to the case of Born-Oppenheimer separation between electronic and vibrational motion for diatomic molecules, nonadiabatic coupling between HSA states is almost always strong and cannot be neglected. Nevertheless, many key features of the dynamics can easily be identified and qualitatively studied. The HSA curves obtained for A_1 vibrational symmetry and $J = 0$ are shown in Fig. 2. At small values of hyperradius, near $\rho = 4.2$, the lowest HSA curves have a minimum, which corresponds to the O_3 equilibrium. Each of the lowest HSA curves near the minimum represents approximately a particular combination of v_2 and v_3 vibrational modes of O_3 . The v_1 mode near the O_3 equilibrium is represented by the continuous variable ρ , which is at this first step not quantized in the space of HSA coordinates. Therefore, the lowest HSA curve $U_a(\rho)$ ($a = 1$) near $\rho = 4.2$ is an adiabatic representation of the set $(\rho, 0, 0)$ of vibrational modes of O_3 corresponding to the normal mode quantum numbers $v_2 = v_3 = 0$, the second and third HSA curves are $(v_2 = 1, v_3 = 0)$ and $(v_2 = 2, v_3 = 0)$,

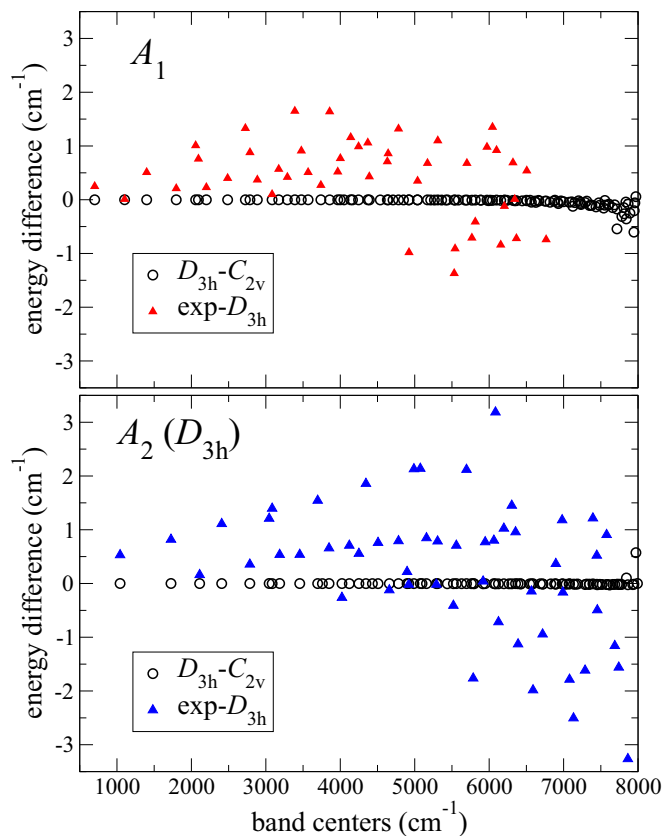


FIG. 3. Comparison of the energies of band centers obtained in this study with the previous calculation [64] and experimental data [8,15–18,67–72] for two vibrational symmetries (A_1 and A_2 in the D_{3h} group employed here, A_1 and B_1 in the C_{2v} group employed in Ref. [64]). The difference between the present results and the previous calculation and experimental data is labeled as $D_{3h}-C_{2v}$ and $\text{exp}-D_{3h}$, respectively.

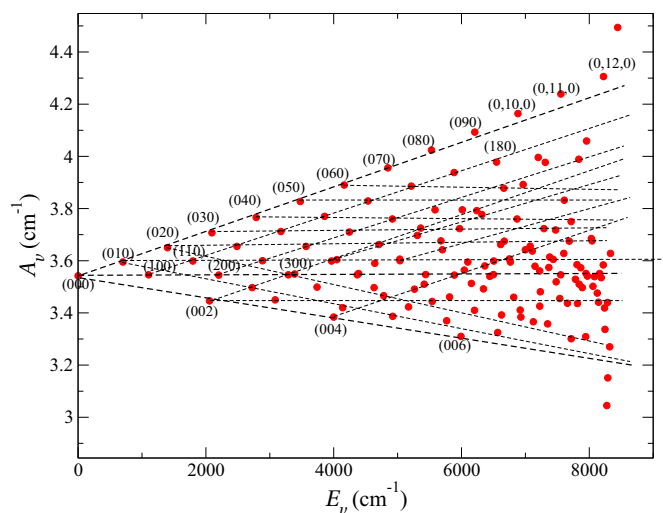


FIG. 4. The largest of the three rotational constants for A_1 vibrational states in the D_{3h} group. Almost linear dependence of the rotational constant A_v on the energy of the vibrational states permits an assignment of normal modes for low energy levels. Normal mode quantum numbers are specified for a few levels. Note that at high energy the normal mode assignment becomes “nominative” and is to be taken with caution because of strong anharmonic basis state mixing.

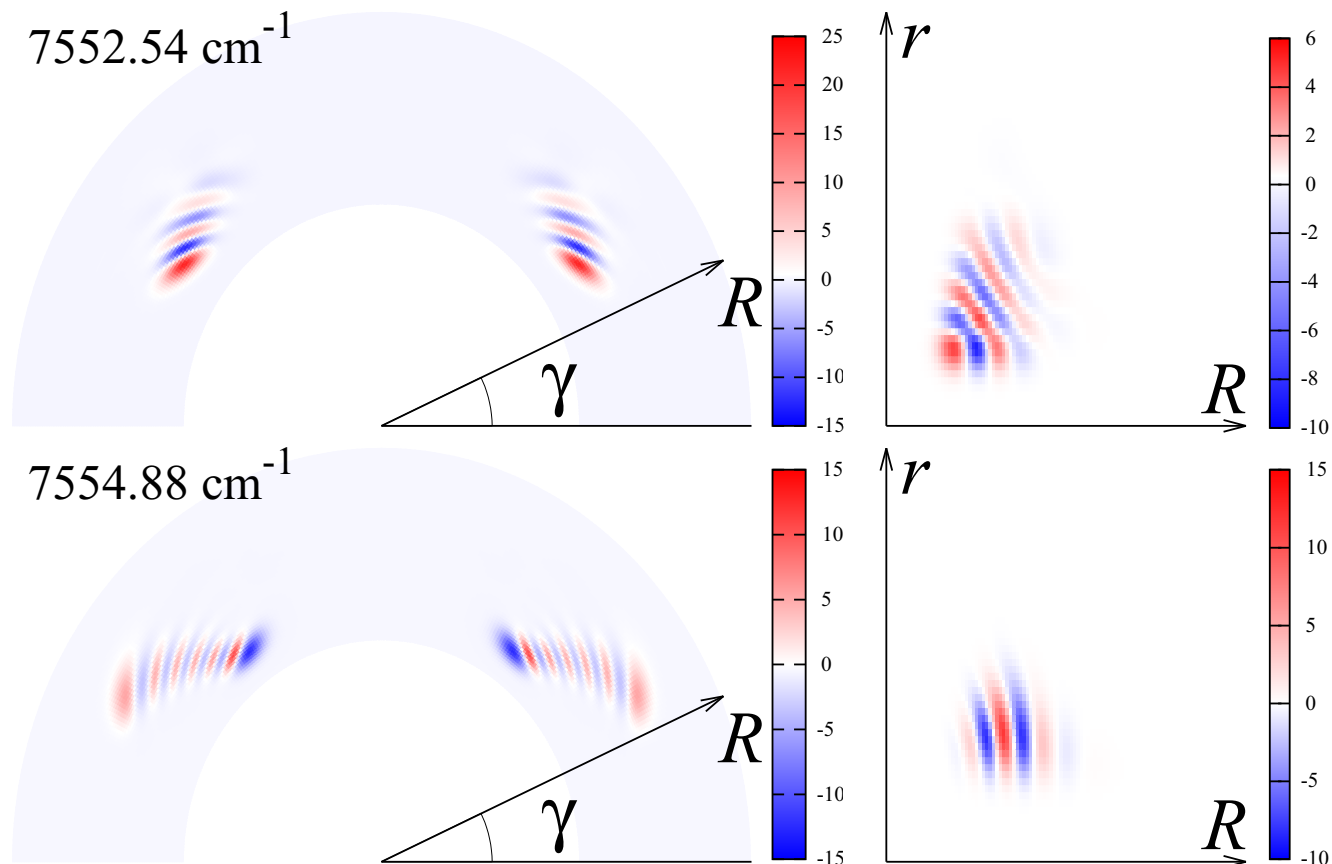


FIG. 5. Wave functions of the (7,0,0) (top panels) and the (0,11,0) (bottom panels) levels as functions of the Jacobi coordinates R , r , and γ . Only the vibrational (without the rotational) part of the wave functions is given. In the left panels, the dependence on R and γ is shown for a fixed value of $r = 2.28a_0$, which is the equilibrium nuclear distance in the O_2 molecule. The right panels show the R, r dependence for fixed $\gamma = 40^\circ$.

the fourth one is ($v_2 = 0, v_3 = 2$), etc. Odd v_3 are not present in A_1 vibrational symmetry.

At energies near and higher than 6000 cm^{-1} above the (0,0,0) level, the normal modes are significantly mixed and the mode assignment becomes more difficult. However, the HSA curves at large energies, above the energy of dissociation, and at large ρ , provide a convenient description of dissociation dynamics. At large ρ , each adiabatic curve converges to a particular asymptotic channel represented by a rovibrational level (v_d, j) of O_2 and the partial wave of relative motion of O_2 and O. As one can see, there are multiple very sharp avoided crossings, especially in the zone of transition from short to large ρ .

IV. BOUND STATES NEAR D_0 AND PREDISSOCIATED RESONANCES

A series of calculations with different parameters of the numerical approach were performed to assess the uncertainty of the obtained energies with respect to the numerical procedure. The final results for A_1 and A_2 vibrational levels were obtained with 60 HSA states. The number of B splines used for each of the hyperspherical angles θ and ϕ was 120. Similar to previous work by Alijah and Kokoouline on the H_3^+ molecule [79], the interval of variation of φ was from $\pi/6$ to $\pi/2$ in calculations of

A_1 and A_2 levels. The variation interval of ρ was from 2.9 to 16; a variable step width [82,84,94] along the ρ grid was used with 192 grid points. The estimated uncertainty due to the employed numerical method is better than 0.001 cm^{-1} for low vibrational levels and about 0.01 cm^{-1} for levels at around 7500 cm^{-1} above the ground vibrational level. This convergence error is significantly lower than the uncertainties of the ozone PES. Figure 3 compares the energies of $^{16}O_3$ band centers up to 8000 cm^{-1} obtained in this study with the previous calculation [64] and experimental data [8,15–18,67–72]. The rms deviation between the calculation of Ref. [64] in C_{2v} symmetry and the present D_{3h} calculations is of 0.03 cm^{-1} only up to this energy cutoff. This confirms a good nuclear basis set convergence of both methods. The rms (obs-calc) deviation for all vibrational band centers directly observed in high-resolution spectroscopy experiments is 1 cm^{-1} . This is by one order of magnitude better than the accuracy of vibrational calculations using other ozone PESs available in the literature. The uncertainty in the determination of resonance energies depends on their widths and is roughly 10% of the respective width. The uncertainty in calculated widths is better than 20% for most of the resonances.

The assignment of vibrational bands is simplified by using the vibrational dependence of rotational constants predicted from the PES and derived from rovibrational spectra analyses

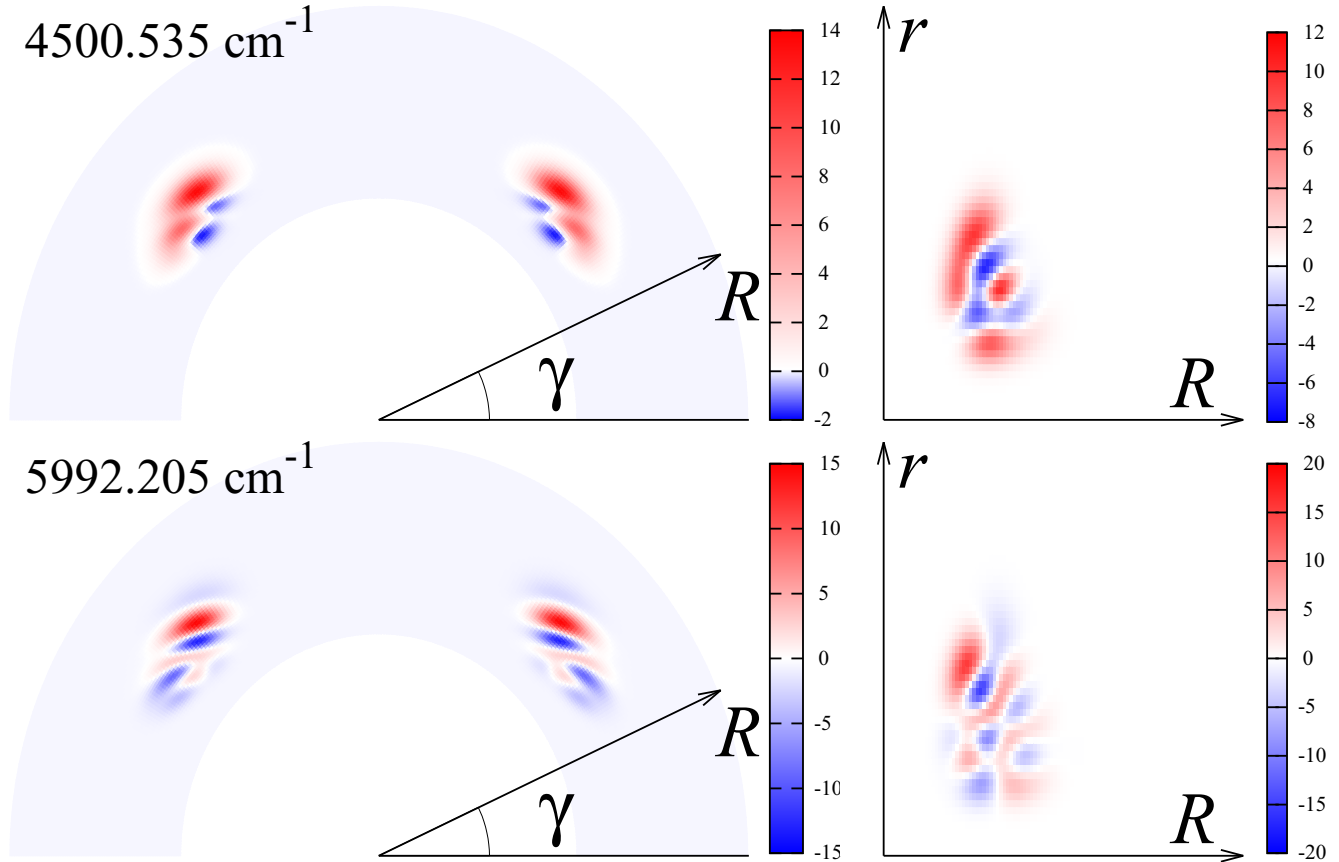


FIG. 6. As Fig. 5, but for the pure antisymmetric stretching modes (0,0,4) (top panels) and (0,0,6) (bottom panels).

as described in Refs. [16,67–71,73]. The largest rotational constant, A_v , corresponding to the “linearization” z axis, is given by the following expression in hyperspherical coordinates [95]:

$$A_v = \langle \Psi_v^{00} | \frac{1}{\mu \rho^2 (1 - \sin \theta)} | \Psi_v^{00} \rangle. \quad (13)$$

At low vibrational excitations, the rotational constant A_v has nearly linear behavior with respect to the normal mode quantum numbers, v_1 , v_2 , or v_3 , with proportionality coefficients different for each mode. This can be seen in Fig. 4. For example, when $v_1 = v_3 = 0$, the levels (0, v_2 , 0) form almost a straight line in the $A_v(E_v)$ plot. The same is true for other series, (v_1 , 0, 0), (0, 0, v_3), (1, v_2 , 0), etc. Near the dissociation limits, the normal mode approximation is not valid anymore and the series become mixed, although the (v_1 , 0, 0) and (0, v_2 , 0) series survive even above the dissociation. Such states cannot dissociate into $O_2 + O$ unless mixed with the antisymmetric vibrational mode.

Figures 5 and 6 and the top panel of Fig. 7 show wave functions of five bound vibrational levels of A_1 vibrational symmetry in terms of Jacobi coordinates R , r , and γ , where r is the distance between two oxygen nuclei of a chosen pair, R is the distance from the center of mass of this pair to the third nucleus, and γ is the angle between the vectors along r and R . The left panels of the figures demonstrate the dependence of the wave functions on R and γ . The interval of variation of γ is from 0° to 180° , such that it covers two of the three

possible equivalent arrangements (permutations) of the three nuclei; i.e., it represents two of the three potential wells of the ozone potential. As evident, the obtained wave functions are symmetric with respect to an exchange between the two wells. Since the calculations were performed in hyperspherical coordinates, the wave functions are also symmetric with respect to the exchange involving the third well, but the Jacobi coordinates cannot easily represent such a symmetry.

To demonstrate the nature of wave functions of different normal modes, the functions chosen in Figs. 5–7 represent “pure” vibrational modes: (7, 0, 0), (0, 11, 0), (0, 12, 0), (0, 0, 4), and (0, 0, 6). It is easy to identify the pure v_1 (symmetric stretching) and v_2 (bending) modes by counting nodes in the Jacobi coordinates, but the behavior of the antisymmetric stretching mode v_3 is more complicated in Jacobi coordinates.

For the calculation of states above the dissociation threshold D_0 , a complex absorbing potential (CAP) and variable grid step along ρ adapted to the local de Broglie wavelength were used as described in Ref. [83]. The parameters of the CAP were chosen to absorb the outgoing dissociation flux for the interval of energies approximately between 100 and 4000 cm^{-1} . When the method of CAP is used, the spectrum of the Hamiltonian matrix for energies above the dissociation limit contains not only the relatively long-living resonance states but also nonphysical “box states.” Real and imaginary parts of box-state eigenvalues depend on the CAP and grid parameters. A manual separation of resonances and box states is difficult for this case because of a large number of resonances. Several calculations

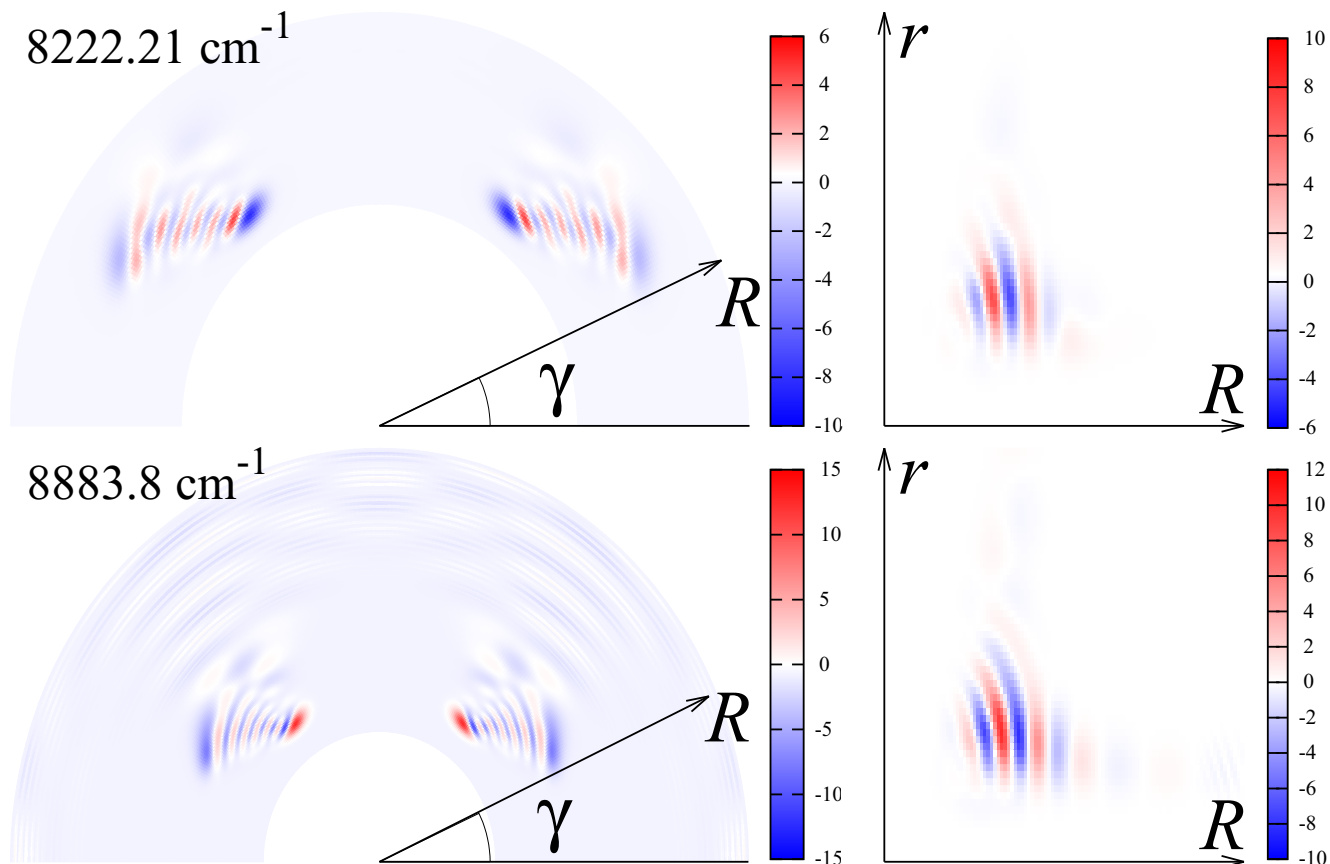


FIG. 7. As Fig. 5, but for the (0, 12, 0) bound (top panels) and (0, 13, 0) resonance (bottom panels) vibrational states. The interval or variation of R in the left-panel plots is larger than in Figs. 5 and 6 in order to demonstrate the long-range tail of the wave functions. Note that the state shown in the lower figure exists only if rotation is excited. Thus, the wave functions are just the vibrational parts of the total rovibrational functions.

with variable parameters, such as CAP, the number of grid points along ρ , the number of the HSA states, and the number of B splines in the HSA calculations, were performed. Spectra obtained with different sets of parameters were compared, allowing us to separate the box states from the resonances, as the latter do not depend on the numerical parameters in a converged calculation.

The bottom panel of Fig. 7 gives an example of a resonance wave function of A_1 vibrational symmetry. As discussed above, such $J = 0$ levels are not allowed for $^{16}\text{O}_3$, at least in the isolated ground electronic PES approximation, but we will consider them because the same analysis can be applied to other isotopologues of O_3 , and also because a similar behavior can be exhibited by A_1 vibrational factors of rotationally excited A_2 states which are allowed for $^{16}\text{O}_3$. At short distances, the resonance is mainly described by the (0, 13, 0) normal mode contribution. Its wave function looks very similar to that of the (0, 12, 0) state. It is still bound but has one more node along the ν_2 coordinate. The outgoing dissociative flux is clearly visible in the R, γ plot. The contrast in the R, r plot is not quite sufficient to see the flux clearly. The vibrational resonance (0, 13, 0) corresponds to large-amplitude bending motion of ozone. The energy of such bending oscillations is above dissociation, but the system does not dissociate fast, because the $\text{O}_2 + \text{O}$ dissociation implies

that two of the three internuclear distances should become very large and the third distance should stay small, whereas when

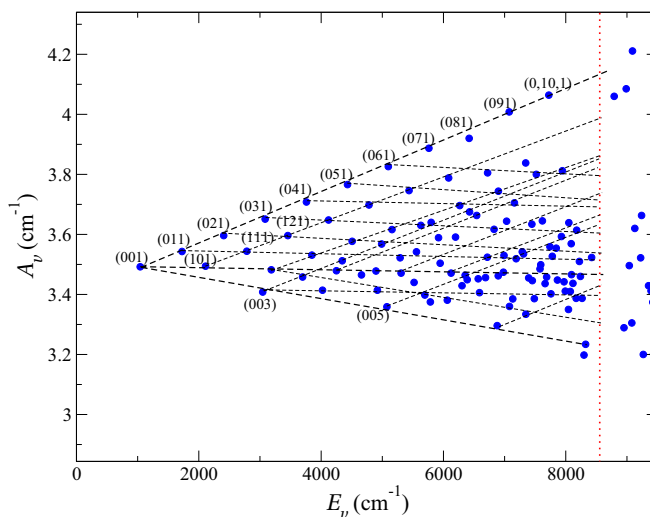


FIG. 8. The A_v rotational constants for $A_2(D_{3h})$ vibrational states. Normal mode quantum numbers are specified for a few levels. Above the dissociation threshold (vertical dotted red line), the vibrational levels are predissociated.

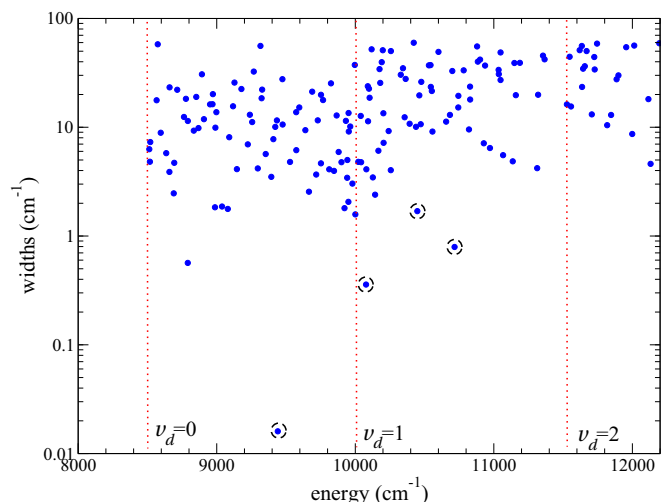


FIG. 9. Widths, Γ , of resonances of the $A_2(D_{3h})$ vibrational levels. Vertical dotted lines indicate threshold energies for dissociation channels with different excitation of the oxygen molecule $v_d = 0, 1$, and 2. Numerically, lifetimes τ in ps are related to the widths in cm^{-1} as $\tau[\text{ps}] = (2\pi c\Gamma [\text{cm}^{-1}])^{-1}$, where c is the speed of light in units of cm/ps , $c = 0.029\,979\,245\,8 \text{ cm}/\text{ps}$. Wave functions of the encircled levels are shown in Figs. 11 and 12.

the molecule oscillates in the v_2 or the v_1 modes, all three internuclear distances increase simultaneously.

Figure 8 shows the vibrational dependence of the rotational constants A_v obtained for A_2 vibrational symmetry in the $D_{3h}(M)$ group. The energy origin of the figure is the same as in Fig. 4, i.e., the energy of the ground rovibrational level of ozone $(0,0,0), J = 0$. The same three families of vibrational levels corresponding to the three normal modes, are easily identified. The figure also includes some of the low-energy predissociated resonances above the dissociation limit. Figure 9 shows widths of the A_2 vibrational levels situated above the dissociation threshold. Most of the resonances shown in the figure have widths between 2 and 70 cm^{-1} (lifetimes between 0.08 and 2 ps) with a few outliers having significantly smaller widths. These outliers are the levels highly excited in the v_1 mode, as demonstrated in Figs. 11 and 12.

Figures 10–12 show some of the bound and resonance vibrational levels of A_2 vibrational symmetry of the D_{3h} group. The vibrational levels (v_1, v_2, v_3) with odd v_3 have overall A_2 symmetry. As mentioned above, continuum states (including dissociative states) of ozone $^{16}\text{O}_3$ can only be of A_2 vibrational symmetry. Figure 11 demonstrates two resonance wave functions from the $(v_1, 0, 1)$ series. Although excitation of the v_1 mode differs for these two levels only by one quantum, their lifetimes are very different: 330 ps for the $(8, 0, 1)$ and 3.1 ps for the $(9, 0, 1)$ level. Figure 12 shows two examples of wave functions for levels where all three modes are excited and mixed.

Figure 13 shows the energies of symmetry-allowed levels for the two lowest values of the angular momentum, $J = 0$ and

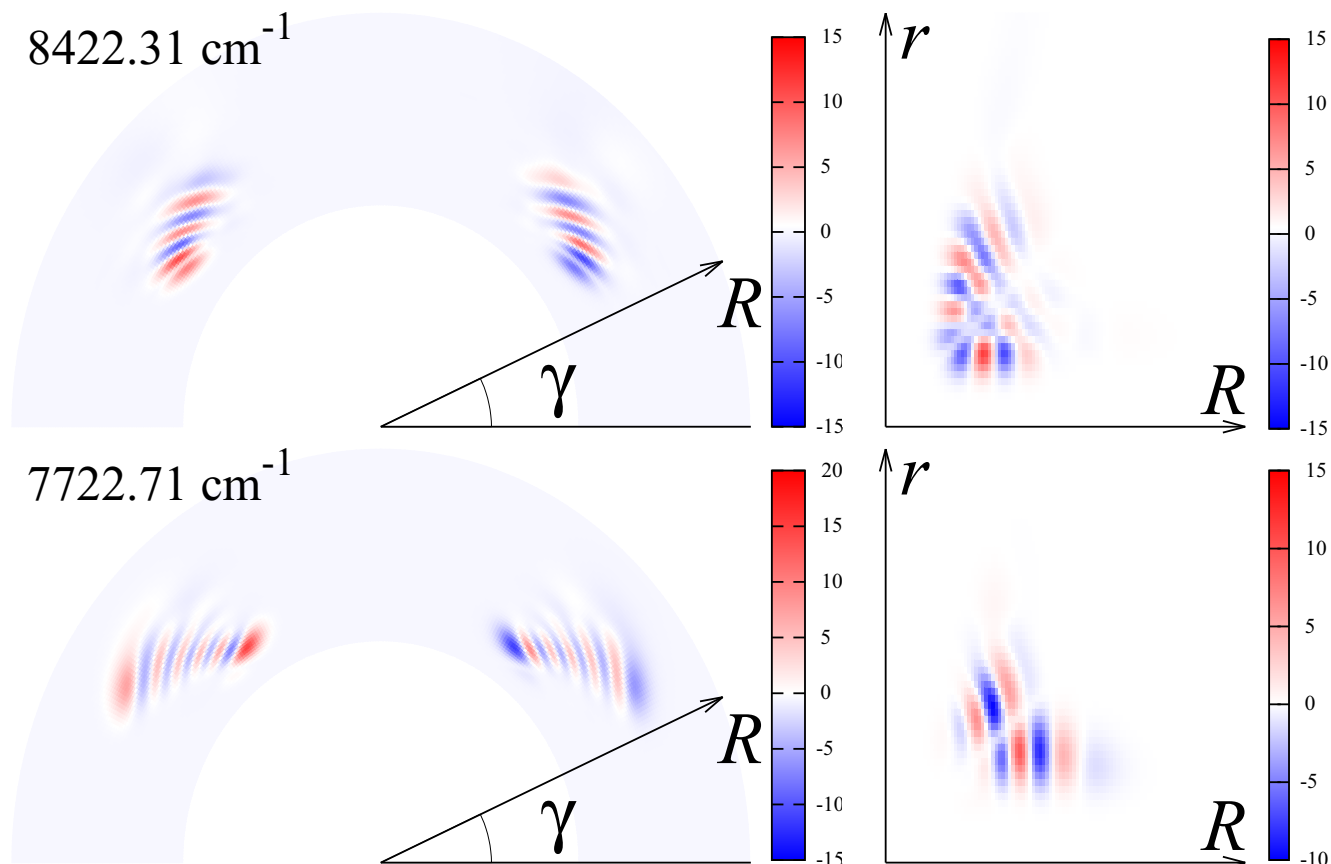


FIG. 10. Same as Fig. 5, but for the $(7,0,1)$ and $(0,10,1)$ wave functions, of $A_2(D_{3h})$ overall vibrational symmetry.

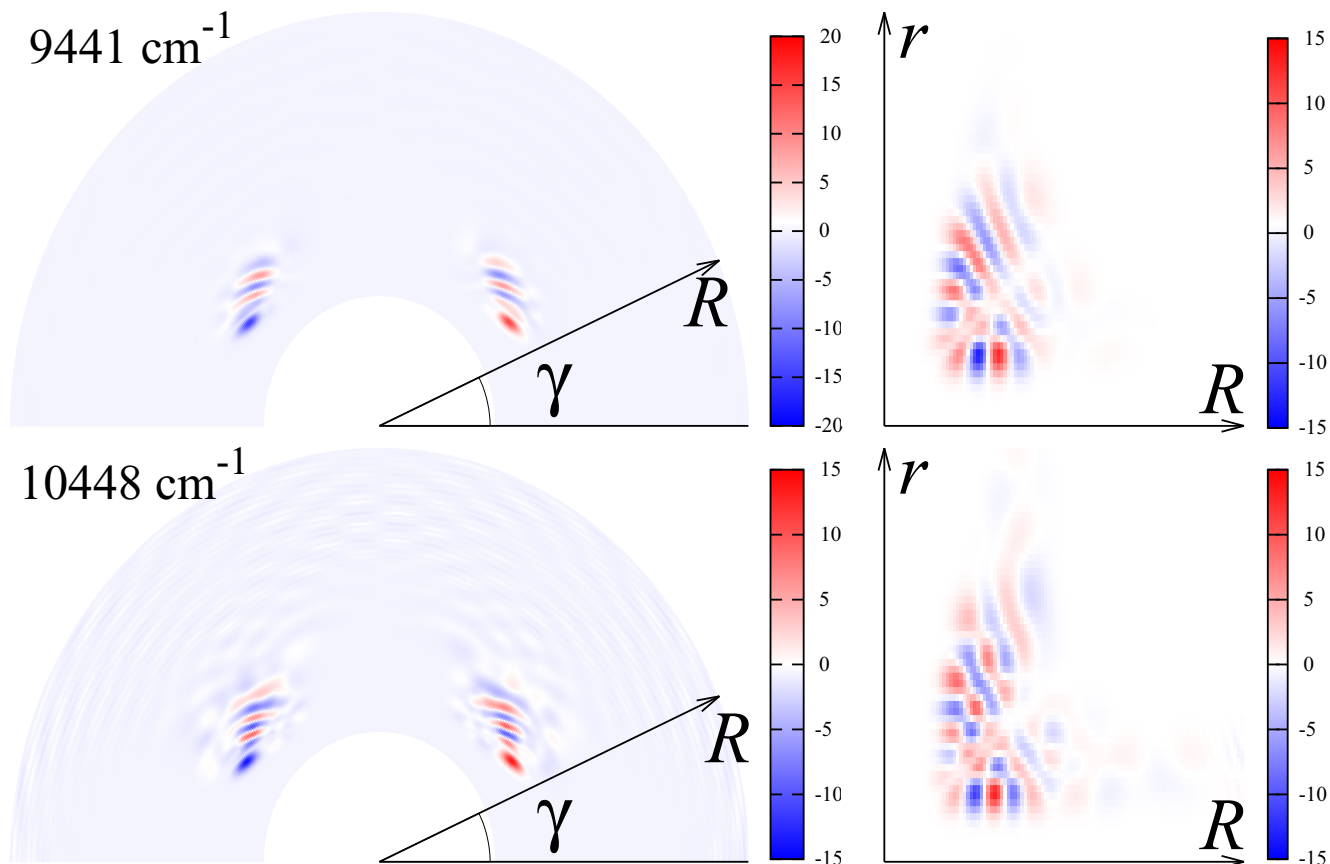


FIG. 11. Vibrational part of the wave functions of the (8,0,1) (top panels) and (9,0,1) (bottom panels) levels of $A_2(D_{3h})$ vibrational symmetry. The calculated widths are $\Gamma = 0.016 \text{ cm}^{-1}$ for the (8,0,1) level and 1.7 cm^{-1} for (9,0,1).

1. The standard notation notation $\{J_{K_a K_c}\}$ for rotational states of an asymmetric top molecule is used for bound states within the well. The irreducible representation in the S_3 permutation group of the vibrational part of the total wave function is also specified. Only states of $A_2(D_{3h})$ vibrational irrep can dissociate and, therefore, only resonances of this symmetry are shown in the figure.

V. CONCLUSION

In this study, energies, widths, and wave functions of $^{16}\text{O}_3$ vibrational resonances were determined for levels up to about 3000 cm^{-1} above the dissociation threshold. The predissociated resonances have lifetimes between 0.08 and 2 ps with a few long-living levels. These outliers are levels with the highly excited v_1 and v_2 modes. An example of a long-living state is (8,1,0) $J = 1$ level with the lifetime of 330 ps. Energies of bound states of the ozone isotopologue $^{16}\text{O}_3$ up to the dissociation threshold were also computed. The total permutation inversion symmetry $S_3 \times I$ of the three oxygen atoms was taken into account using hyperspherical coordinates. The effect of the symmetry is negligible for the levels deep in the ozone potential, but vibrational levels near the dissociation threshold cannot be represented correctly within one potential well and, therefore, the complete permutation symmetry group should be used.

Symmetry properties of allowed rovibrational levels of ozone (applicable to $^{16}\text{O}_3$ and $^{18}\text{O}_3$) as well as correlation diagrams between the bound-state and dissociation regions were derived and discussed. The correlation diagrams are not trivial because ozone dissociates to (or is formed from) a P -state oxygen atom and an O_2 molecule of symmetry $^3\Sigma_g^-$.

Within the employed model including only the lowest PES of ozone, the purely vibrational states, i.e., $J = 0$ states, of ozone $^{16}\text{O}_3$ (and $^{18}\text{O}_3$) cannot dissociate to the fragments allowed by symmetry of the electronic ground state of the O_2 molecule. Note that excited rotational states with $J > 0$ satisfying Eq. (3) do exist. Examples of such resonances are shown in Figs. 11 and 12. We would like to stress here that the single electronic PES model neglects the coupling of the angular momentum of the molecular frame, \mathbf{R} , with the electronic angular momentum, \mathbf{L} , which is not zero. In general, the total (but without nuclear spin, \mathbf{I}) angular momentum \mathbf{J} can be written as $\mathbf{J} = \mathbf{R} + \mathbf{L} + \mathbf{S} + \mathbf{\Pi}$, where \mathbf{S} is the electronic spin and $\mathbf{\Pi}$ the vibrational angular momentum. From this we obtain the approximate quantum number of the rotation of the molecular frame as $\mathbf{R} = \mathbf{J} - \mathbf{L} - \mathbf{S} - \mathbf{\Pi}$. Neglecting the effect of \mathbf{L} and \mathbf{S} in the rovibrational problem, $\mathbf{R} \approx \mathbf{J}$ is a “good” quantum number. Our rovibrational energies have been calculated within this approximation, as have been those obtained by other workers in the field. However, the importance of the electronic angular momentum is evident from asymptotic behavior of Eq. (3): At large distances

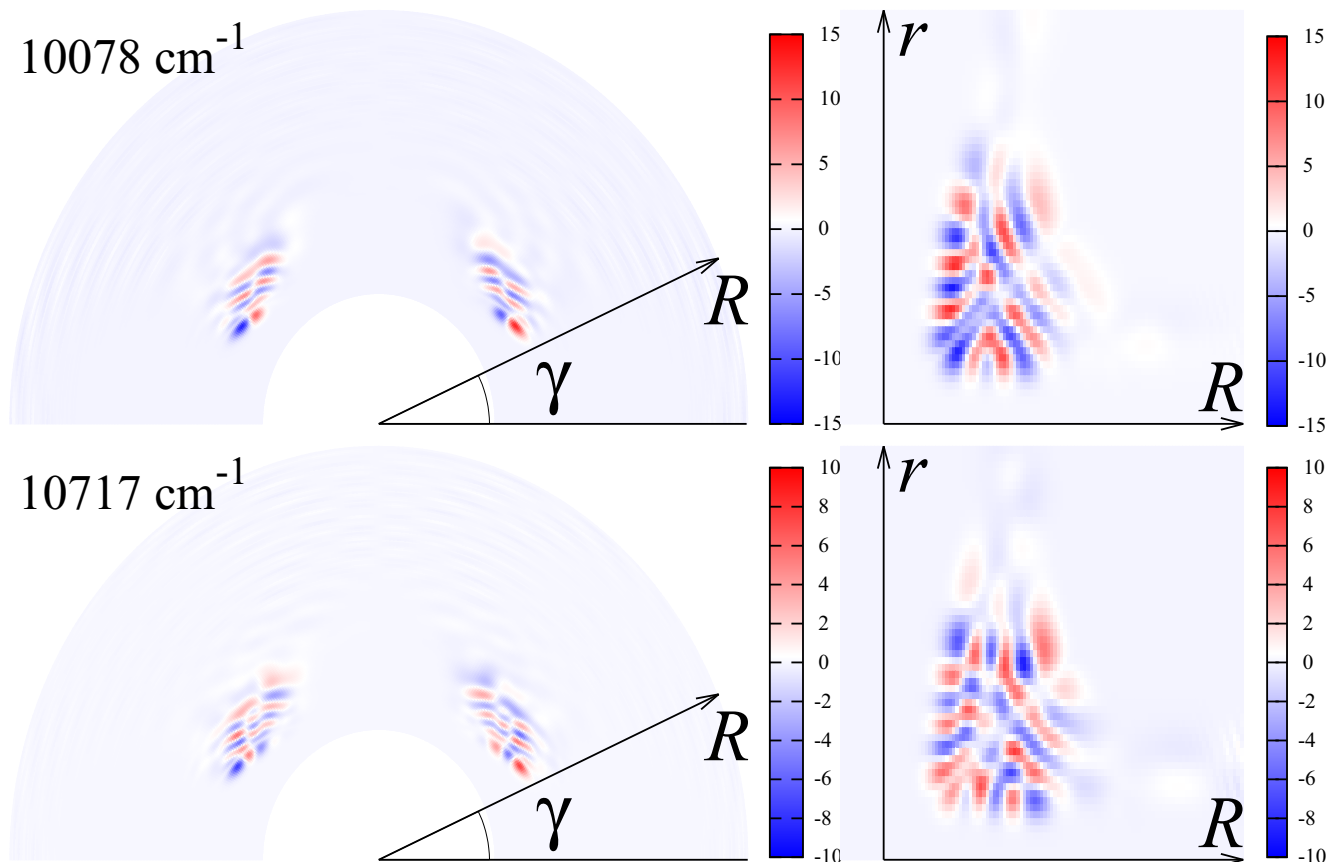


FIG. 12. Vibrational part of the wave functions of two highly excited levels of the $A_2(D_{3h})$ symmetries. They are vibrationally assigned as $(8,1,1)$ and $(8,2,1)$ via the normal mode decomposition using the contact transformation method of Ref. [96]. The calculated widths are $\Gamma = 0.36 \text{ cm}^{-1}$ for the function shown in the top panels and 0.8 cm^{-1} for the function shown in the bottom panels.

between O and O_2 , the electronic angular momentum is clearly not zero. In a more accurate model, the electronic momentum

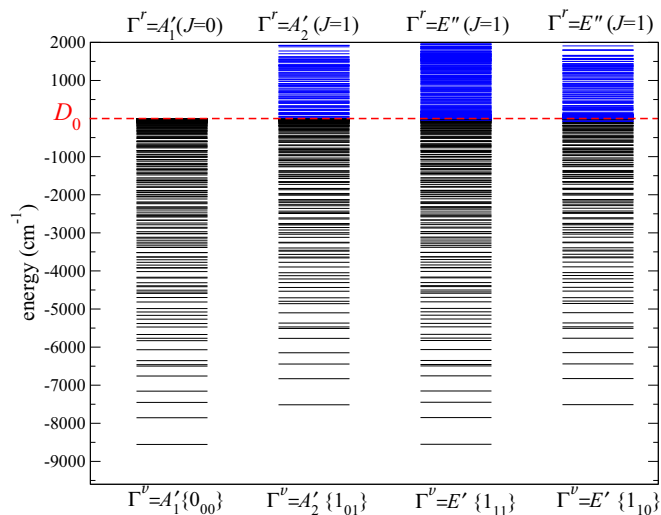


FIG. 13. Energies of vibrational levels for $J = 0$ and $J = 1$. In addition to the symbol $\{J_{K_a}K_c\}$ of the rotational states of an asymmetric top molecule, irreducible representations of the vibrational part (Γ^v , below the graph) and rotation part (Γ^r , above the graph) of the wave function are specified. The corresponding resonances are shown in blue.

should be accounted for and coupled to the angular momentum of the nuclear frame, due to the cross terms generated by R^2 , conserving the total angular momentum, J . In such a more accurate model, the continuum vibrational spectrum for $J \approx R = 0$ is allowed (since R is not “conserved” any more). The corresponding vibrational resonances should have relatively long lifetimes because they can only decay due to non-Born-Oppenheimer and Coriolis couplings involving the three PESs converging to the same dissociation limit, with the oxygen atom being in the triply degenerate electronic state. Such long-living states above the dissociation threshold, for example, $(9,0,0)$ and $(10,0,0)$, have indeed been observed in experiments. Therefore, an accurate theoretical determination of lifetimes of $J = 0$ resonance levels would involve three potential energies surfaces.

A three-state treatment has also been suggested by Garcia-Fernandez *et al.* [9], since there is a conical intersection line at equilateral triangular configurations between the first and the second excited singlet states and an avoided crossing between the ground state and the first excited singlet state. The three C_{2v} minima can be seen as due to Jahn-Teller stabilization through vibronic distortion of the equilateral configurations. The Jahn-Teller stabilization energy, i.e., the energy difference between the minimum of the conical intersection and the C_{2v} minima, is very big, $\approx 77600 \text{ cm}^{-1}$, which means that the minimum of the intersection is located high in the continuum of

the electronic ground state. Nevertheless, the intersection gives rise to a topological geometrical phase whose inclusion affects the statistical weights of the computed vibrational states, as we have demonstrated for the case of triplet H_3^+ [79], where the Jahn-Teller stabilization energy is about $18\,000\text{ cm}^{-1}$ and the minimum of the conical intersection about $15\,000\text{ cm}^{-1}$ above dissociation. However, the role of the geometrical phase in ozone is more complicated, as there is evidence for further conical intersections [97,98], which add to the phase factor of the equilateral intersection discussed by Garcia-Fernandez *et al.* and might cancel it. Investigation of the phase factors in ozone will be a subject of future work.

The above discussion did not take into account spin-orbit coupling. For even more realistic description of the nuclear motion states in the continuum, one has to consider the effect of coupling of the electronic singlet state with electronic triplet states, of symmetry B_1 and A_2 in $C_{2v}(M)$, or A_2'' and A_1' in $D_{3h}(M)$, or A'' in $C_s(M)$, that approach the same asymptotic dissociation limit, $O(^3P)$ and $O_2(X^3\Sigma_g^-)$, as the electronic ground state. Rosmus, Palmieri, and Schinke [99] have determined the spin-orbit coupling elements with all relevant triplet states in the asymptotic channel. The matrix elements are of the order of $\langle X^1A_1 | H_{so} | ^3A_2' \rangle \approx 60\text{ cm}^{-1}$. The long-range behavior of the potential energy surfaces accounting for spin-orbit coupling was discussed in Ref. [100].

To study the effect of spin-orbit coupling, the total nuclear-electronic wave function must be expanded, including for simplicity just one generic triplet state, as

$$\Psi_{vJm}(\Omega, \mathcal{Q}) = \sum_k \left[c_1 |^1A_1' \rangle \psi_{vJk;^1A_1'}(\mathcal{Q}) + c_2 |^3A_2' \rangle \psi_{vJk;^3A_2'}(\mathcal{Q}) \right] \mathcal{R}_{Jkm}(\Omega). \quad (14)$$

As before, the product of electronic and nuclear motion functions must have the same symmetry as the rotational function, except for their parity. However, the nuclear motion component of the $^3A_2'$ electronic state is antisymmetric and

can therefore correlate with the asymptotic $O_2 + O$ wave function. A full treatment of the nuclear dynamics of ozone accounting for the spin-orbit coupling would involve solving the rovibrational Schrödinger equation on several coupled potential energy surfaces, which is hardly possible at present. However, an adiabatic approach with respect to the spin-orbit coupling should also be accurate and could be used in a future study. In the approach, the first step would be to construct the matrix of the potential energy. The matrix would include the lowest three Born-Oppenheimer PESs, mentioned above, and the spin-orbit coupling such as described in Refs. [99,100]. The matrix then should be diagonalized for each geometry, which will produce adiabatic potential surfaces accounting for the spin-orbit coupling. Because the lowest Born-Oppenheimer PES (X^1A_1) does not cross the two other PESs at energies near or below the dissociation threshold, after the diagonalization, the lowest obtained PES will be very similar to the original X^1A_1 Born-Oppenheimer PES, except that the dissociation limit will be shifted down. Low-energy rovibrational states obtained with the new adiabatic PES will be almost identical to the ones discussed in this study. States near the dissociation threshold (approximately 60 cm^{-1} above and below D_0) will have energies somewhat different compared to the ones obtained with the PES without the spin-orbit coupling. However, qualitatively the structure of rovibrational levels near the dissociation will stay the same.

ACKNOWLEDGMENTS

This work is supported by the CNRS through an invited professor position for V. K. at the GSMA, the National Science Foundation, Grant No. PHY-15-06391 and the ROMEO HPC Center at the University of Reims Champagne-Ardenne. The supports from Tomsk State University Academic D. Mendeleev funding Program, from French LEFE Chat program of the Institut National des Sciences de l'Univers (CNRS), and from Laboratoire International Franco-Russe SAMIA are acknowledged.

-
- [1] R. Schinke, S. Y. Grebenshchikov, M. Ivanov, and P. Fleurat-Lessard, *Annu. Rev. Phys. Chem.* **57**, 625 (2006).
- [2] R. A. Marcus, *Proc. Natl. Acad. Sci. USA* **110**, 17703 (2013).
- [3] M. V. Ivanov and D. Babikov, *Proc. Natl. Acad. Sci. USA* **110**, 17708 (2013).
- [4] Z. Sun, L. Liu, S. Y. Lin, R. Schinke, H. Guo, and D. H. Zhang, *Proc. Natl. Acad. Sci. USA* **107**, 555 (2010).
- [5] Y. Li, Z. Sun, B. Jiang, D. Xie, R. Dawes, and H. Guo, *J. Chem. Phys.* **141**, 081102 (2014).
- [6] T. R. Rao, G. Guillon, S. Mahapatra, and P. Honvault, *J. Phys. Chem. Lett.* **6**, 633 (2015).
- [7] S. Y. Grebenshchikov, Z.-W. Qu, H. Zhu, and R. Schinke, *Phys. Chem. Chem. Phys.* **9**, 2044 (2007).
- [8] V. G. Tyuterev, R. Kochanov, A. Campargue, S. Kassi, D. Mondelain, A. Barbe, E. Starikova, M. R. De Backer, P. G. Szalay, and S. Tashkun, *Phys. Rev. Lett.* **113**, 143002 (2014).
- [9] P. Garcia-Fernandez, I. B. Bersuker, and J. E. Boggs, *Phys. Rev. Lett.* **96**, 163005 (2006).
- [10] F. A. L. Mauguière, P. Collins, Z. C. Kramer, B. K. Carpenter, G. S. Ezra, S. C. Farantos, and S. Wiggins, *J. Chem. Phys.* **144**, 054107 (2016).
- [11] Q.-B. Lu, *Phys. Rev. Lett.* **102**, 118501 (2009).
- [12] A. Boynard, C. Clerbaux, P.-F. Coheur, D. Hurtmans, S. Turquety, M. George, J. Hadji-Lazaro, C. Keim, and J. Meyer-Arneke, *Atmos. Chem. Phys.* **9**, 6255 (2009).
- [13] J.-M. Flaud, C. Camy-Peyret, C. P. Rinsland, M. A. H. Smith, and V. M. Devi, *Atlas of Ozone Spectral Parameters from Microwave to Medium Infrared* (Academic Press, San Diego, CA, 1990).
- [14] S. Mikhailenko, A. Barbe, V. G. Tyuterev, L. Regalia, and J. Plateaux, *J. Mol. Spectrosc.* **180**, 227 (1996).
- [15] A. Campargue, S. Kassi, D. Romanini, A. Barbe, M.-R. De Backer-Barilly, and V. G. Tyuterev, *J. Mol. Spectrosc.* **240**, 1 (2006).
- [16] A. Barbe, S. Mikhailenko, E. Starikova, M.-R. D. Backer, V. Tyuterev, D. Mondelain, S. Kassi, A. Campargue, C. Janssen,

- S. Tashkun, R. Kochanov, R. Gamache, and J. Orphal, *J. Quant. Spectrosc. Radiat. Transfer* **130**, 172 (2013).
- [17] D. Mondelain, R. Jost, S. Kassı, R. H. Judge, V. Tyuterev, and A. Campargue, *J. Quant. Spectrosc. Radiat. Transfer* **113**, 840 (2012).
- [18] Y. L. Babikov, S. N. Mikhailenko, A. Barbe, and V. G. Tyuterev, *J. Quant. Spectrosc. Radiat. Transfer* **145**, 169 (2014).
- [19] L. Xiao and M. E. Kellman, *J. Chem. Phys.* **90**, 6086 (1989).
- [20] Y. Q. Gao and R. Marcus, *Science* **293**, 259 (2001).
- [21] Y. Q. Gao and R. Marcus, *J. Chem. Phys.* **116**, 137 (2002).
- [22] D. Charlo and D. C. Clary, *J. Chem. Phys.* **120**, 2700 (2004).
- [23] T. Xie and J. M. Bowman, *Chem. Phys. Lett.* **412**, 131 (2005).
- [24] M. R. Wiegell, N. W. Larsen, T. Pedersen, and H. Egsgaard, *Int. J. Chem. Kinet.* **29**, 745 (1997).
- [25] R. Schinke, P. Fleurat-Lessard, and S. Y. Grebenshchikov, *Phys. Chem. Chem. Phys.* **5**, 1966 (2003).
- [26] S. Y. Lin and H. Guo, *J. Chem. Phys. A* **110**, 5305 (2006).
- [27] A. L. Van Wyngarden, K. A. Mar, K. A. Boering, J. J. Lin, Y. T. Lee, S.-Y. Lin, H. Guo, and G. Lendvay, *J. Am. Chem. Soc.* **129**, 2866 (2007).
- [28] E. Vetoshkin and D. Babikov, *Phys. Rev. Lett.* **99**, 138301 (2007).
- [29] S. Y. Grebenshchikov and R. Schinke, *J. Chem. Phys.* **131**, 181103 (2009).
- [30] R. Dawes, P. Lolur, J. Ma, and H. Guo, *J. Chem. Phys.* **135**, 081102 (2011).
- [31] K. Mauersberger, *Geophys. Res. Lett.* **8**, 935 (1981).
- [32] D. Krankowsky and K. Mauersberger, *Science* **274**, 1324 (1996).
- [33] C. Janssen, J. Guenther, D. Krankowsky, and K. Mauersberger, *Chem. Phys. Lett.* **367**, 34 (2003).
- [34] M. H. Thiemens and J. E. Heidenreich, *Science* **219**, 1073 (1983).
- [35] H. Hippler, R. Rahn, and J. Troe, *J. Chem. Phys.* **93**, 6560 (1990).
- [36] K. Luther, K. Oum, and J. Troe, *Phys. Chem. Chem. Phys.* **7**, 2764 (2005).
- [37] S. Y. Grebenshchikov, *Few-Body Syst.* **45**, 241 (2009).
- [38] D. Babikov, B. K. Kendrick, R. B. Walker, R. T. Pack, P. Fleurat-Lesard, and R. Schinke, *J. Chem. Phys.* **119**, 2577 (2003).
- [39] C. Janssen and R. Marcus, *Science* **294**, 951 (2001).
- [40] G. Guillon, T. R. Rao, S. Mahapatra, and P. Honvault, *J. Phys. Chem. A* **119**, 12512 (2015).
- [41] S. A. Ndengué, R. Dawes, F. Gatti, and H.-D. Meyer, *J. Chem. Phys. A* **119**, 12043 (2015).
- [42] S. A. Ndengué, R. Dawes, and F. Gatti, *J. Phys. Chem. A* **119**, 7712 (2015).
- [43] S. S. Xantheas, G. J. Atchity, S. T. Elbert, and K. Ruedenberg, *J. Chem. Phys.* **94**, 8054 (1991).
- [44] R. Siebert, R. Schinke, and M. Bittererová, *Phys. Chem. Chem. Phys.* **3**, 1795 (2001).
- [45] R. Siebert, P. Fleurat-Lessard, R. Schinke, M. Bittererová, and S. Farantos, *J. Chem. Phys.* **116**, 9749 (2002).
- [46] A. Kalemios and A. Mavridis, *J. Chem. Phys.* **129**, 054312 (2008).
- [47] F. Holka, P. G. Szalay, T. Müller, and V. G. Tyuterev, *J. Phys. Chem. A* **114**, 9927 (2010).
- [48] T. Shiozaki and H.-J. Werner, *J. Chem. Phys.* **134**, 184104 (2011).
- [49] G. Atchity and K. Ruedenberg, *Theor. Chem. Acc.* **96**, 176 (1997).
- [50] P. Hay, R. Pack, R. Walker, and E. Heller, *J. Phys. Chem.* **86**, 862 (1982).
- [51] A. Banichevich, S. D. Peyerimhoff, and F. Grein, *Chem. Phys.* **178**, 155 (1993).
- [52] R. Hernandez-Lamoneda, M. R. Salazar, and R. Pack, *Chem. Phys. Lett.* **355**, 478 (2002).
- [53] R. Schinke and P. Fleurat-Lessard, *J. Chem. Phys.* **121**, 5789 (2004).
- [54] P. Fleurat-Lessard, S. Y. Grebenshchikov, R. Siebert, R. Schinke, and N. Halberstadt, *J. Chem. Phys.* **118**, 610 (2003).
- [55] S. Y. Grebenshchikov, R. Schinke, P. Fleurat-Lessard, and M. Joyeux, *J. Chem. Phys.* **119**, 6512 (2003).
- [56] M. Joyeux, S. Y. Grebenshchikov, J. Bredenbeck, R. Schinke, and S. C. Farantos, *Adv. Chem. Phys.* **130**, 267 (2005).
- [57] D. Babikov, *J. Chem. Phys.* **119**, 6554 (2003).
- [58] H.-S. Lee and J. C. Light, *J. Chem. Phys.* **120**, 5859 (2004).
- [59] R. Dawes, P. Lolur, A. Li, B. Jiang, and H. Guo, *J. Chem. Phys.* **139**, 201103 (2013).
- [60] W. Xie, L. Liu, Z. Sun, H. Guo, and R. Dawes, *J. Chem. Phys.* **142**, 064308 (2015).
- [61] Z. Sun, D. Yu, W. Xie, J. Hou, R. Dawes, and H. Guo, *J. Chem. Phys.* **142**, 174312 (2015).
- [62] S. Ndengué, R. Dawes, X.-G. Wang, T. Carrington, Jr., Z. Sun, and H. Guo, *J. Chem. Phys.* **144**, 074302 (2016).
- [63] M. Ayouz and D. Babikov, *J. Chem. Phys.* **138**, 164311 (2013).
- [64] V. G. Tyuterev, R. V. Kochanov, S. A. Tashkun, F. Holka, and P. G. Szalay, *J. Chem. Phys.* **139**, 134307 (2013).
- [65] B. Ruscic, R. E. Pinzon, M. L. Morton, N. K. Srinivasan, M.-C. Su, J. W. Sutherland, and J. V. Michael, *J. Phys. Chem. A* **110**, 6592 (2006).
- [66] B. Ruscic, available at atct.anl.gov.
- [67] D. Mondelain, A. Campargue, S. Kassı, A. Barbe, E. Starikova, M.-R. De Backer, and V. G. Tyuterev, *J. Quant. Spectrosc. Radiat. Transfer* **116**, 49 (2013).
- [68] E. Starikova, A. Barbe, D. Mondelain, S. Kassı, A. Campargue, M.-R. De Backer, and V. G. Tyuterev, *J. Quant. Spectrosc. Radiat. Transfer* **119**, 104 (2013).
- [69] M.-R. De Backer, A. Barbe, E. Starikova, V. G. Tyuterev, D. Mondelain, S. Kassı, and A. Campargue, *J. Quant. Spectrosc. Radiat. Transfer* **127**, 24 (2013).
- [70] A. Barbe, M.-R. De Backer, E. Starikova, X. Thomas, and V. G. Tyuterev, *J. Quant. Spectrosc. Radiat. Transfer* **149**, 51 (2014).
- [71] E. Starikova, A. Barbe, M.-R. De Backer, V. G. Tyuterev, D. Mondelain, S. Kassı, and A. Campargue, *J. Quant. Spectrosc. Radiat. Transfer* **149**, 211 (2014).
- [72] A. Campargue, S. Kassı, D. Mondelain, A. Barbe, E. Starikova, M.-R. De Backer, and V. G. Tyuterev, *J. Quant. Spectrosc. Radiat. Transfer* **152**, 84 (2015).
- [73] E. Starikova, D. Mondelain, A. Barbe, V. G. Tyuterev, S. Kassı, and A. Campargue, *J. Quant. Spectrosc. Radiat. Transfer* **161**, 203 (2015).
- [74] Here we use a common abbreviation for the ozone isotopologues: 666 \equiv (^{16}O)₃, 668 \equiv $^{16}\text{O}^{16}\text{O}^{18}\text{O}$, 686 \equiv $^{16}\text{O}^{18}\text{O}^{16}\text{O}$, etc.
- [75] H. Longuet-Higgins, *Mol. Phys.* **6**, 445 (1963).
- [76] P. R. Bunker and P. Jensen, *Molecular Symmetry and Spectroscopy* (NRC Research Press, Ottawa, Ontario, Canada, 1998).

- [77] It is important here to note that no degenerate representations are included in the molecular symmetry group $D_{\infty h}(M)$, in contrast to the point group $D_{\infty h}$, which contains representations of type Π , Δ , etc. The order of the group $D_{\infty h}(M)$ is four, while that of the point group $D_{\infty h}$ is infinite.
- [78] This choice is different from that of Bunker and Jensen [76]. As a result, the symmetry labels B_1 and B_2 are interchanged.
- [79] A. Aljiah and V. Kokoouline, *Chem. Phys.* **460**, 43 (2015).
- [80] V. Kokoouline and C. H. Greene, *Phys. Rev. A* **68**, 012703 (2003).
- [81] N. Douguet, J. Blandon, and V. Kokoouline, *J. Phys. B: At. Mol. Opt. Phys.* **41**, 045202 (2008).
- [82] V. Kokoouline and F. Masnou-Seeuws, *Phys. Rev. A* **73**, 012702 (2006).
- [83] J. Blandon, V. Kokoouline, and F. Masnou-Seeuws, *Phys. Rev. A* **75**, 042508 (2007).
- [84] J. Blandon and V. Kokoouline, *Phys. Rev. Lett.* **102**, 143002 (2009).
- [85] B. R. Johnson, *J. Chem. Phys.* **73**, 5051 (1980).
- [86] B. R. Johnson, *J. Chem. Phys.* **79**, 1906 (1983).
- [87] B. R. Johnson, *J. Chem. Phys.* **79**, 1916 (1983).
- [88] V. Kokoouline and C. H. Greene, *Phys. Rev. A* **69**, 032711 (2004).
- [89] S. Fonseca dos Santos, V. Kokoouline, and C. H. Greene, *J. Chem. Phys.* **127**, 124309 (2007).
- [90] R. C. Whitten and F. T. Smith, *J. Math. Phys.* **9**, 1103 (1968).
- [91] B. D. Esry, Many-body Effects in Bose-Einstein Condensates of Dilute Atomic Gases, Ph.D. thesis, University of Colorado, 1997.
- [92] O. I. Tolstikhin, S. Watanabe, and M. Matsuzawa, *J. Phys. B: At. Mol. Opt. Phys.* **29**, L389 (1996).
- [93] I. Tuvi and Y. B. Band, *J. Chem. Phys.* **107**, 9079 (1997).
- [94] V. Kokoouline, O. Dulieu, R. Kosloff, and F. Masnou-Seeuws, *J. Chem. Phys.* **110**, 9865 (1999).
- [95] V. Kokoouline and C. H. Greene, *Faraday Discuss.* **127**, 413 (2004).
- [96] V. Tyuterev, S. Tashkun, M. Rey, R. Kochanov, A. Nikitin, and T. Delahaye, *J. Phys. Chem. A* **117**, 13779 (2013).
- [97] D. Theis, J. Ivanic, T. L. Windus, and K. Ruedenberg, *J. Chem. Phys.* **144**, 104304 (2016).
- [98] L. De Vico, L. Pegado, J. Heimdal, P. Söderhjelm, and B. O. Roos, *Chem. Phys. Lett.* **461**, 136 (2008).
- [99] P. Rosmus, P. Palmieri, and R. Schinke, *J. Chem. Phys.* **117**, 4871 (2002).
- [100] M. Lepers, B. Bussery-Honvault, and O. Dulieu, *J. Chem. Phys.* **137**, 234305 (2012).